Analytical theory of the hydrophobic effect of solutes in water

Tomaz Urbic and Ken A. Dill

Phys. Rev. E **96**, 032101 — Published 1 September 2017

DOI: 10.1103/PhysRevE.96.032101

An analytical theory of the hydrophobic effect of solutes in water

Tomaz Urbic*

University of Ljubljana, Faculty of Chemistry and Chemical Technology,

Večna pot 113, SI-1000 Ljubljana, Slovenia

Ken A. Dill

Laufer Center for Physical and Quantitative Biology,

Stony Brook University, Stony Brook, NY 11794-5252

Abstract

We develop an analytical statistical-mechanical model for hydrophobic solvation in water. In this 3-dimensional Mercedes-Benz-like model, two neighboring waters have three possible interaction states: a radial van der Waals interaction, a tetrahedral orientation-dependent hydrogen-bonding interaction, or no interaction. Nonpolar solutes are modeled as van der Waals particles of different radii. The model is sufficiently simple that we can calculate the partition function and thermal and volumetric properties of solvation vs. temperature, pressure and solute radius. Predictions are in good agreement with results of Monte Carlo simulations. And, their trends agree with experiments on hydrophobic solute insertion. The theory shows that first-shell waters are more highly structured than bulk waters, because of hydrogen bonding, and that that structure melts out faster with temperature than it does in bulk waters. Because the theory is analytical, it can explore a broad range of solvation properties and anomalies of water, at minimal computational expense.

* tomaz.urbic@fkkt.uni-lj.si

I. INTRODUCTION

The solvation properties of the nonpolar molecules in water is sufficiently peculiar that it is given its own name, *hydrophobic effect*[1–5]. These unusual behaviors are particularly reflected in the enthalpies, entropies, heat capacities, and volumes of transfer of such solutes into water [1–3]. It has long been of interest to interpret these observations in terms of the structures and energies of individual water molecules – their hydrogen bonding, tetrahedrality, etc. So, a substantial body of work has sought structure-property relationships using atomistic potentials with explicit-solvent models sampled by Molecular Dynamics (MD) or Monte Carlo (MC) computer simulations[6–8].

An alternative route to insights is through coarser-grained analytical theory [9–11]. The evident downside is that coarse-graining throws away some details of molecular structure. Those details might matter. However, analytical theories also offer some advantages: (1) They can be much faster to compute. So, a single study (such as the present one) can explore how solvation depends on temperature and pressure and solute radius and solute energy parameters all at the same time, without large computing resources. (2) Analytical models are particularly good for exploring principles. In analytical theories, there can be tight logical linkages from molecular structure to observable properties. Parameters can be varied – much more readily than in atomistic simulations – to test how the macroscopic properties arise from microscopic structures. (3) Analytical models often give the best basis for engineering models, where there is a need to express observed behaviors fairly accurately with a minimum number of physical parameters. (4) And, even the disadvantage – that some details of molecular structure must be left out of the model – can actually be an advantage, because they provide an opportunity to explore which details matter, and which don't. Here, we give an analytical model of the hydrophobic effect; it builds upon earlier work by Luksic et al [12].

Hydrophobic hydration has some interesting aspects. Solvation thermodynamics in simpler systems is determined by an unfavorable enthalpy change of dissolution. But dissolving nonpolar solutes in water has a favorable enthalpy of transfer ($\Delta H_{TR} < 0$) (i.e. enthalpy for the process of transferring non-polar particle from vacuum to bulk water) at low temperatures. Dissolving oil in water is unfavorable ($\Delta G_{TR} > 0$) due to the negative entropy of transfer $\Delta S_{TR} < 0$ [1, 2]. Also unusual is the observation that both the enthalpy and

entropy change strongly with temperature. This fact is summarized by stating that the heat capacity of transfer is high and positive ($\Delta C_{p,TR} \gg 0$), since

$$\Delta C_{p,TR} = \frac{d\Delta H_{TR}}{dT} = T\frac{d\Delta S_{TR}}{dT}, \tag{1}$$

where T is temperature. These features are known as the hydrophobic effect [1–3, 13–19]. There have been many models for how hydrophobic solvation depends on solute size. Among the first, scaled particle theory (SPT) estimates the work necessary to create a spherical cavity in water [5, 20]. It successfully predicts the free energy of small cavity formation and was constructed to give the surface tension of water in the planar limit. However, SPT has been criticized for predicting a monotonic increase in the entropy penalty of transfer with increasing cavity size and an incorrect temperature dependence in the surface tension [5]. Stillinger was perhaps the first to suggest that water solvates large nonpolar molecules differently than small molecules [5]. Pratt and Chandler developed an integral equation method that used pair correlations of bulk waters to predict the solubilities of small solutes [21]. The theory of Lum, Chandler, and Weeks [17] reduces to Pratt-Chandler theory for small solutes but predicts large-scale drying as predicted by Stillinger near larger nonpolar surfaces[5]. The hydrophobic effect plays an important role in many common processes in nature (e.g. protein folding, ligand binding) and technology (e.g. micelle formation). So, it has been extensively studied experimentally [22–26]. Hydrophobic solvation as a function of solute size has also been studied in computer simulations using explicit and implicit water models. A key conclusion from such simulations is that at planar nonpolar surfaces water will waste a hydrogen bond by pointing the bond directly at the surface, in contrast to small nonpolar surfaces, where water conserves hydrogen bonds by pointing those bonds in directions that straddle the solute. Explicit models (such as TIP or SPC) can be computationally expensive, precluding the calculation of full temperature or pressure dependencies. And, computer simulation results are, in general, susceptible to large statistical errors, causing difficulties in determining certain quantities accurately, such as the heat capacity [27, 28]. Implicit models are faster, but the trade-off is sometimes physical inaccuracies. There exist also many other water-like models that were used for treating hydrophbic effect. Core softened [29] or Jagla fluids [30] possess water-like structural, dynamic, and thermodynamic anomalies and these fluids also display water-like solvation thermodynamics. Another aspect of structure-based coarse-graining relies on matching the pair correlation functions of

a reference (atomistic) and coarse-grained system [31, 32]. It was demonstrated that it can be generalized for inhomogeneous systems as well as solvation. Coarse-gaining performed in inhomogeneous systems improves thermodynamic properties and the structure of interfaces without significant alterations to the local structure of the bulk liquid.

Here, we adapt a Mercedes-Benz-like model of water, which has previously been studied in 2D and 3D[9–11] to study the 3D hydration of a nonpolar solute. The idea behind the model originated with Ben-Naim in the 1970s [33–36]. Recently, it has been developed further by Bizjak et al.[27, 37] and Dias et al.[38, 39], and studied using computer simulations [27, 37–39] and integral equation theory[37]. The MB models of water are toy models that have the advantage of explaining in a simple way interplay of thermodynamic properties and the angle dependent potential, but cannot be used for qualitative prediction of properties. The analytical theories for MB-like models allow the inclusion of orientation-dependent hydrogen bonding within a framework that is simple and nearly analytical. According to 3D MB model, each water molecule is a Lennard–Jones sphere with four arms, oriented tetrahedrally to mimic formation of hydrogen bonds. In a statistical mechanical model, which is based on 2D Urbic and Dill's (UD) model being directly descendant from a treatment of Truskett and Dill (TD), who developed a nearly analytical version of the 2D MB model [41, 42], each water molecule interacts with its neighboring waters through a van der Waals interaction and an orientation-dependent interaction that models hydrogen bonds. A related analytical treatment was developed by Coronas et al. [43] and was also studied by Monte Carlo simulations. It is a coarse-grained model for bulk water that includes many-body interactions associated with water cooperativity. It possesses water-like anomalies and the liquid-liquid phase transition also present in our analytical treatment of water. The main difference between the two models is that in our energy is a continuous function of the relative orientation θ of two water molecules while in the other the HB energy is a discontinuous function of the relative configurations, but both models possess similar features. For hydrophobic hydration, Xu and Dill [44] proposed a very simple analytical theory of the hydrophobic effect in 2D which builds on a two-dimensional Mercedes–Benz model of water. Starting from the statistical partition functions for a water molecule in the bulk and a water in the first solvation shell around a hydrophobe, the theory reproduces the main characteristics of the hydrophobic effect and it accounts for different solute size effects. The theory of Xu and Dill [44] required the results of a reference Monte Carlo simulation of pure

bulk water phase. That approach was improved by Luksic et al [12], which is simpler and circumvents any computer simulation steps by using an analytical model of the pure phase of water. Both solvation methods were for 2D cases. In this work, we applied theory to 3D MB model of water. In addition to moving the theory to 3D, we implement additional improvements by assuming that water properties in the first solvation shell change due to higher density because of interaction between water and solute. The new version of the theory can be used in all liquid regions of the 3D MB model, including the super-cooled region where computer simulations can not obtain solvation properties due to crystallization and convergence problems.

Here, we start from an analytical 3D UD theory of water [10]. A partition function for a water molecule in the bulk and the first hydration shell of a hydrophobic solute is then built using the expressions for average energies of different states of the water molecule (hydrogen-bonded, van der Waals and open), upon considering the geometric restrictions through which a solute dictates the formation or breakage of the hydrogen bonds between water molecules in the first solvation shell. Finally, from statistical mechanical and thermodynamical relations, we calculate the ΔG, ΔH, $T\Delta S$, and ΔC_p. In order to explore the performance of the analytical theory in describing the hydrophobic hydration we used existing computer simulation data [45, 46] for the simplified water model, a three dimensional version of the Ben-Naim water model (3D MB)[27]. The MB model has previously been shown to capture the essential physics of water, namely van der Waals interaction and hydrogen-bonding, which are essential for hydrophobic hydration [14, 16–18, 28]. Here, we explore the performance of the analytical theory for the dependence of the hydrophobic effect on temperature, pressure, and solute size.

II. 3D MB WATER MODEL

We applied analytical theory to the 3D MB water model where each water molecule is represented as a Lennard-Jones sphere with an additional tetrahedrally-dependent potential that mimics the hydrogen-bonding of true water [27]. The interaction potential between two 3D MB particles is

$$U(\mathbf{X_i}, \mathbf{X_j}) = U_{LJ}^{11}(r_{ij}) + U_{HB}(\mathbf{X_i}, \mathbf{X_j}), \tag{2}$$

where r_{ij} is the distance between centres of particles i and j and $\mathbf{X_i}$ is a vector denoting the position and orientation of particle i. U_{LJ}^{mn} is the standard Lennard-Jones potential

$$U_{LJ}^{mn}(r_{ij}) = 4\varepsilon_{LJ}^{mn}\left(\left(\frac{\sigma_{LJ}^{mn}}{r_{ij}}\right)^{12} - \left(\frac{\sigma_{LJ}^{mn}}{r_{ij}}\right)^{6}\right). \tag{3}$$

where ϵ_{LJ}^{mn} denotes the well-depth and σ_{LJ}^{mn} is the contact parameter. m is 1 if the i^{th} particle is water and 2 the i^{th} particle is a solute and the same goes for n regarding the j^{th} particle. The hydrogen-bonding term is the sum of interactions over all possible pairs of HB arms

$$U_{HB}(\mathbf{X_i}, \mathbf{X_j}) = \sum_{k,l}^{4} U_{HB}^{kl}(r_{ij}, \mathbf{\Omega_i}, \mathbf{\Omega_j}), \tag{4}$$

where $U_{HB}^{k,l}$ is the interaction between HB arms k and l on two particles and vector $\mathbf{\Omega_i}$ denotes the orientation of particle i. The interaction between two HB arms of different particles is

$$U_{HB}^{kl}(r_{ij}, \mathbf{\Omega_i}, \mathbf{\Omega_j}) = \epsilon_{HB} G(r_{ij} - r_{HB}) G(\mathbf{i_k u_{ij}} - 1) G(\mathbf{j_l u_{ij}} + 1). \tag{5}$$

Here $\mathbf{u_{ij}}$ is the unit vector pointing from particle i to particle j, $\mathbf{i_k}$ is the unit vector representing arm k on particle i. Between vector $\mathbf{u_{ij}}$ and vectors representing the orientations of arms there is dot product. $G(x)$ is the unnormalized Gaussian function (requirement that $G(0) = 1$)

$$G(x) = e^{-x^2/2\sigma^2}. \tag{6}$$

The model does not distinguish between hydrogen-bond donors and acceptors. The width of the Gaussian function for distance and angles is the same ($\sigma = 0.085$) and was chosen to be small enough that a direct hydrogen bond is more favorable than a bifurcated one [27, 37]. It regards two waters as being hydrogen bonded when their Hbond arms are collinear with each other. The strongest hydrogen-bond is formed when two arms are pointing towards each other particles' centers when the centers are separated by r_{HB} [27, 38, 39]. In the following section we will first summarize the theory for pure 3D MB and explain how parameters of the model for analytical theory are extracted from continuous potential presented in this section.

III. THEORY

A. The model for the pure water reference state

The structure of the liquid state is modeled as a variation of the cell model theory and is a perturbation from a hexagonal (ice) lattice (see Figure 1). One grid point is occupied by only one molecule. Our focus is on a single water molecule and its interactions with the neighboring molecule. The interaction between a pair of molecules can be one of the three possibilities. Note that in our theory we limit interactions from the continuous one to only the three most probable interactions, minimas in energy as function of distance for HB and LJ interactions and no interaction. We say that each water molecule can be in one of three possible orientational states relative to its clockwise-like positioned neighbor on the lattice: (i) hydrogen-bonded (HB) state, (ii) van der Waals (LJ) state, or (iii) non-bonded (NB) state. This is presented in Figure 2. First we compute the isothermal-isobaric statistical weights, Δ_i, of the states as a functions of temperature, pressure, and interaction energies [9–11].

In the HB state the test water molecule can point one of its four hydrogen bonding arms at an angle θ to within $\pi/3$ of the center of its neighbor water. This is an approximation and was determined by the condition that one quarter of the total solid angle is occupied per hydrogen bond and to keep calculations of integrals analytical. In this case it forms a hydrogen bond[10, 11] (see Figure 2) and the interaction energy of the test water with its neighbor is then described by this equation

$$u_{HB}(\theta) = -\epsilon_{HB} + k_s(1-\cos\theta)^2, 0 < \theta < \pi/3. \tag{7}$$

ϵ_{HB} is an HB energy constant of the maximal strength of a HB and k_s is the angular spring constant that describes the weakening of the hydrogen bond with angle. This is a type of hydrogen bond that is called a weak bond [9] because it does not cooperate with neighboring hydrogen bonds. The isothermal-isobaric partition function, Δ_{HB}, of this state is calculated by integrating this Boltzmann factor over all angles ϕ, θ and ψ and over all the separations x, y and z of the test molecule relative to its clockwise neighbor. In the vdW state, the test water molecule forms a contact with its clockwise-like positioned water, but it does not form any hydrogen bond. Energy of this state can be written as

$$u_{LJ}(\theta) = -\epsilon_{LJ}, \tag{8}$$

The isothermal-isobaric partition function, Δ_{LJ}, of this state is obtained using the same integration as for the HB state. In the last NB state, the test water molecule does not interact with its neighbor so the energy is equal to zero

$$u_0(\theta) = 0. \tag{9}$$

By knowing the isobaric-isothermal ensemble partition functions for each state we can write the partition function Q_1 for a full single hexagon of 6 waters as

$$Q_1 = (\Delta_{HB} + \Delta_{LJ} + \Delta_o)^6, \tag{10}$$

If we include also higher cooperativity in ice [9–11] we can write the total partition function for each hexagon as

$$Q_1 = (\Delta_{HB} + \Delta_{LJ} + \Delta_o)^6 - \Delta_{HB}^6 + \delta\Delta_s^6. \tag{11}$$

$\delta = \exp(-\beta\epsilon_c)$ is the Boltzmann factor for the cooperativity energy, ϵ_c, that applies only when 6 water molecules all collect together into a full hexagonal cage. The terms on the righthandside of this expression simply replace the statistical weight for each weakly hydrogen-bonded full hexagonal cage with the statistical weight for a cooperative strongly hydrogen-bonded hexagonal cage. Δ_s is the Boltzmann factor for a cooperative hexagonal cage. It differs from Δ_{HB} only in the volume per molecule, v_s instead of v_{HB} [9–11]. Now we combine the Boltzmann factors for the individual water molecules to get the partition function for the whole system of N particles. The population of different states f_j can be calculated [9–11] and all the other thermodynamic properties from simple derivations of the partition function as described previously [9–11, 41, 42]. The attraction beyond pair terms is treated in the mean-field attractive level with energy [40], $-Na/v$, among hexagons, where a is the van der Waals dispersion parameter [9, 41, 42] and v is the average molar volume. Parameters needed for calculations can be obtained directly from the interaction pair potential between two 3D MB water particles (ϵ_{HB}=1, r_{HB}=1, ϵ_{LJ}=0.1, σ_{LJ}=0.7)[27, 37] or from analyzing the angle and distance dependence of the 3D MB potential in comparison with the potential used in analytical theory (k_s=80, a=0.045, ϵ_c=0.18).

For modeling the solvation of a nonpolar solute, it is necessary to summarize volumes and to calculate additional quantities. Volumes of the states are [10, 11]

$$v_s = \frac{8\sqrt{3}r_{HB}^3}{9} \tag{12}$$

$$v_{HB} = \frac{v_s}{x_v} \tag{13}$$

$$v_{LJ} = \sigma_{LJ}^3 \tag{14}$$

$$v_o = \frac{k_B T}{p} + v_{LJ} \tag{15}$$

The $x_v = 2.5$ is chosen empirically to get the proper behavior of the density dependence in the original water papers [10, 11]. The ensemble average energy, $\langle u_j \rangle$, for each of the three types of water molecule structures, can be calculated as

$$\langle u_j \rangle = \frac{\int_0^{\pi/3} u_j \sin\theta d\theta \exp\left(-(u_j + p v_j/2)/k_B T\right)}{\int_0^{\pi/3} \sin\theta d\theta \exp\left(-(u_j + p v_j/2)/k_B T\right)}\,. \tag{16}$$

Integration gives us

$$\langle u_{\rm HB} \rangle = -\epsilon_{\rm HB} + \frac{kT}{2} - \frac{\sqrt{\frac{k_{\rm s} kT}{4\pi}} \exp\left(-\frac{k_{\rm s}}{4kT}\right)}{\mathrm{erf}\left(\sqrt{\frac{k_{\rm s}}{4kT}}\right)} \tag{17}$$

$$\langle u_{\rm S} \rangle = \langle u_{\rm HB} \rangle + \frac{\epsilon_{\rm c}}{6} \tag{18}$$

$$\langle u_{\rm LJ} \rangle = -\epsilon_{\rm LJ} \tag{19}$$

$$\langle u_0 \rangle = 0. \tag{20}$$

The average energy $\langle u_S \rangle$ is obtained by adding 1/6 of the correlation energy to $\langle u_{HB} \rangle$. The average energy of a water molecule, summed over the four different water states, can be expressed as

$$\langle \epsilon \rangle_{\rm b} = 2\left(\langle u_{\rm HB} \rangle f_{\rm HB} + \langle u_{\rm S} \rangle f_{\rm S} + \langle u_{\rm LJ} \rangle f_{\rm LJ}\right). \tag{21}$$

B. The model for inserting a nonpolar solute into water

To develop the theory for the solvation of nonpolar solutes, we followed same steps as in Luksic et al [12]. A nonpolar solute molecule of diameter $\sigma_{\rm s}$ is inserted into water. Now we consider what happens with two water molecules in the first hydration shell of

the solute (see Figure 3.). The presence of the solute imposes a geometric restriction since a solvation-shell water molecule may be unable to form all four hydrogen bonds with its neighboring waters as in the bulk. Let $\zeta(\phi, \theta, \psi)$ be the maximum number of hydrogen bonds the water in the first solvation shell can form for a specific orientation. ϕ, θ, ψ are Euler angles describing the orientation of a water molecule in the first solvation shell and $\zeta(\phi, \theta, \psi)$ is also a function of the solute radius. There are different possibilities depending on the size of the solute molecule. For smaller solutes, water molecules in the first solvation shell can form a maximum of either 3 or 4 hydrogen bonds depending on the orientation. For bigger solutes, first-shell water molecules can form a maximum of only 1, 2 or 3 hydrogen bonds. A critical angle ϕ_{c} is defined as angle at which a hydrogen-bonding arm points along a tangent to the solute (see Figure 3) and both waters are in the Lennard-Jones minimum

$$\phi_{\mathrm{c}} = \arccos \frac{r_{\mathrm{HB}}}{(\sigma_{\mathrm{s}} + \sigma_{\mathrm{LJ}})\sqrt[6]{2}}\,. \tag{22}$$

This is the angle where water can still form a hydrogen bond. A similar definition of this angle was used by Chaimovich and Shell in their work [47, 48]. Integration over all possible orientations of water (over all 3 Euler angles) is equal to $8\pi^2$. The next step is to determine the ratio of orientations of water molecules that can form 4, 3, 2 or 1 hydrogen bond. Note that water can always forms at least one hydrogen bond in the first solvation shell. Ratios can be determined by sampling over orientations of water in first solvation shell and counting the number of hydrogen bonds water can form. This gives us ratios of orientations ζ_i where water can form i hydrogen bonds. A solute molecule does not impose just geometric restrictions on first-shell water molecules, but it also perturbs the energetics of water-water interactions in the first shell. Water's density in the first solvation shell is higher than in the bulk, depending on the value of the attraction between the solute and the water

$$\rho_h = \rho_b \exp{(\beta\epsilon_{SW})}, \tag{23}$$

where $\epsilon_{SW} = \epsilon_{LJ}$ is the minimum of the Lennard-Jones interaction between solute and water. Since we do not have density as input to the analytical theory, we have to calculate properties of water in the first solvation shell by increasing pressure for

$$\Delta p = \frac{\beta\epsilon_{SW}}{\kappa}, \tag{24}$$

where κ is compressibility of bulk water. The populations of waters with different states in the first solvation shell are now different comparing to the bulk and are equal to f_j^{h}. Note

that the average energies of different states stay the same, only populations change. The average energy of a water molecule in the first solvation shell, summed over the four different water states, can be expressed as

$$\langle \epsilon(\phi,\theta,\psi)\rangle_{\rm h} = \frac{1}{2}\left\{\zeta(\phi,\theta,\psi)\left[\langle u_{\rm HB}\rangle f^{\rm h}_{\rm HB} + \langle u_{\rm S}\rangle f^{\rm h}_{\rm S}\right] + 4\langle u_{\rm LJ}\rangle f^{\rm h}_{\rm LJ} - \epsilon_{\rm SW}\right\}, \tag{25}$$

Now we can calculate the partition function of water in the bulk by treating interactions in averaged way, namely

$$\begin{aligned} q_{\rm b} &= \int\int d\phi d\psi \int_0^{\pi/3} \sin\theta d\theta \exp\left(-\frac{\langle\epsilon\rangle_{\rm b} + pv^{\rm b}_{\rm mol}}{kT}\right) \\ &= 8\pi^2 \exp\left(-\frac{\langle\epsilon\rangle_{\rm b} + pv^{\rm b}_{\rm mol}}{kT}\right), \end{aligned} \tag{26}$$

where $v^{\rm b}_{\rm mol}$ is molar volume of bulk water. The partition function for a water molecule in the first shell around a solute molecule can be written as

$$q_{\rm h} = \int\int d\phi d\psi \int_0^{\pi/3} \sin\theta d\theta \exp\left(-\frac{\langle\epsilon\rangle_{\rm h} + pv^{\rm h}_{\rm mol}}{kT}\right), \tag{27}$$

where $v^{\rm h}_{\rm mol}$ denotes the molar volume of water in first solvation shell. It is smaller than the $v^{\rm b}_{\rm mol}$ by the overlap volume Δv ($v^{\rm h}_{\rm mol} = v^{\rm b}_{\rm mol} - \Delta v$) (see Figure 4.) [12]. We compute the Gibbs free energy of transferring a hydrophobic solute into water using [44]

$$\Delta G = -n(\sigma_{\rm s})kT\ln\left(\frac{q_{\rm h}}{q_{\rm b}}\right), \tag{28}$$

where $n(\sigma_{\rm s})$ is the average number of water molecules in the first solvation shell. In this theory we assumed that $n(\sigma_{\rm s})$ is proportional to the solvent surface accessible area of the solute [12]. Standard thermodynamic relations give the enthalpy and the entropy of transfer as

$$\Delta H = n(\sigma_{\rm s})kT^2\frac{\partial\ln\left(q_{\rm h}/q_{\rm b}\right)}{\partial T}, \tag{29}$$

$$T\Delta S = \Delta H - \Delta G \tag{30}$$

IV. PREDICTIONS OF THE THEORY, AND COMPARISONS TO CORRESPONDING MONTE CARLO SIMULATIONS

In this section, we give the theory's predictions for how the hydrophobic effect depends on temperature, pressure, and solute size. The analytical results are compared with the

Monte Carlo simulation results of 3D Mercedes–Benz water by Mohoric et al. [45, 46]. As has been done previously [9–12], we present our results below in dimensionless units, normalized to the strength of the optimal hydrogen bond ϵ_{HB} and hydrogen bond separation r_{HB} ($T^* = k_BT/\epsilon_{HB}$, $u^{ex*} = u^{ex}/\epsilon_{HB}$, $V^* = V/r_{HB}^2$, and $p^* = pr_{HB}^2/\epsilon_{HB}$).

A. Inserting the solute changes the Hbonding of waters in the first solvation shell relative waters in the bulk

First, we show the 4 types of water populations (6-water-cages, 2-water Hbonded, vdW, and nonbonded) of pure bulk water, with no solute, as a function of temperature; see Figure 5. This figure allows us to establish the approximate ranges over which the model acts like, ice, cold liquid water, hot liquid water, and vapor. Our main interest here is in exploring solvation across the range from cold liquid to hot liquid, where solvation anomalies are most pronounced. This range of anomalies is best represented in this model by the supercooled region of the pT phase diagram reported in previous work [11] where we reported that the 3D MB model exhibits two critical points; the liquid-gas critical point (C1) at T^*_{C1}=0.1166, p^*_{C1}=0.0115, ρ^*_{C1}=0.467 and the liquid-liquid critical point (C2) at T^*_{C2}=0.0779, p^*_{C2}=0.167, ρ^*_{C2}=1.295. There exists also a region of pressures between both critical points where we have only one fluid phase, at higher pressures we have two liquid phases, and at lower pressures the liquid and the gas phases. So, while we cannot draw a precise correspondence with true ambient p and T values, Figure 5 shows that we can approximately regard the model as having ice-like behavior below about $T^* = 0.1$, cold liquid water up to about $T^* = 0.1-0.15$, hot liquid water up to about $T^* = 0.15 - 0.2$, and vapor above about $T^* = 0.25$.

Then, in the following sections below, we show that the analytical model reproduces fairly well the temperature dependences of the free energy, enthalpy, entropy and volumes from the underlying model, as determined by Monte Carlo simulations. This is just a validation of the analytical theory against the Monte Carlo simulations. Then, in the last section, we show how the model's thermal and volumetric behaviors are explained by the underlying microscopic water populations.

B. The thermal and volumetric properties of solvation are captured by the theory

Figure 6 shows the transfer free energy, ΔG^*, as a function of temperature for different sizes of hydrophobic particles ($\sigma_S^* = \sigma_{LJ}^{22}/r_{HB}$). For large solutes, see Figure 6a; for small ones, see Figure 6b. The symbols represent the results of the computer simulations and the lines are the results of the analytical theory. In general, the analytical theory gives good agreement with the simulations. We observe a qualitative difference between small and large hydrophobes. Bigger positive transfer free energies on these plots indicates increasing unfavorability for inserting the solute from vapor into water. The difference is only for very small solutes (smaller than size of a water molecule); in that case, inserting a small solute into hot water is favorable (ΔG^* is negative). These results are in agreement with the experimental observation for the thermodynamics of hydration of argon [2], and show qualitative differences from the behavior of ΔG^* for larger hydrophobes. Increasing the solute size increases the unfavorability of dissolving in water. The analytical theory correctly captures these subtle differences.

Figure 7 shows the enthalpy and entropy of solute transfer from vacuum into water, ΔH^*, and transfer entropy, $T^*\Delta S^*$, for different solute sizes. Both functions first increase, and then decrease with temperature, as observed experimentally [2]. The agreement between the computer simulation results (symbols) and analytical theory (lines) is quite good in the whole temperature range studied, even for the large solutes. Transfer enthalpies are positive for large solutes since solute insertion into water requires breaking water-water bonds, and since the interaction with the solute does not contribute sufficient energy to compensate. For small solutes, transfer enthalpies are negative since small molecules are inserted into empty spaces within the water structure and there is no hydrogen bond breaking required for insertion. The transfer entropy is most positive when waters in the first solvation shell have the highest density. Analytical theory also predict unexpected behavior at low temperatures where transfer enthalpy and entropy increase upon decreasing the temperature. Simulation data are not available in this range due to convergence problems, so we can not verify if this is a failure of the theory or not.

Figure 8 shows how the volume ΔV^* of the whole system (solute plus solvent) changes as a solute is inserted into water as a function of temperature and for different solute sizes. The analytical theory gives trends that are consistent with experiments, showing that for

relatively small solutes, ΔV^* increases with temperature [23]. The main contribution to the transfer volume is the size of the nonpolar solute, then upon increase of temperature water become more gas like and there is more empty space around solutes, which gives additional increase of transfer volume.

C. The theory gives correct trends of solvation thermodynamics vs. solute size

Figure 9 summarizes the dependence of the solvation free energy, enthalpy, and entropy on the solute radius. Again, there is good general consistency with the simulations for most solute sizes. The disagreement is bigger for larger solutes, especially for entropy transfer. The reason might be in problems within the theory or bad computer simulation data which authors calculated by Widom's insertion method which is problematic for insertion of large particles. The solvation free energy for large solutes increases linearly with area, while for small solutes it increases linearly with volume [14, 17, 19]. For small solutes, the entropy contribution to the change in free energy dominates ($T\Delta S > \Delta H$), but for larger solutes, $T\Delta S < \Delta H$. Figure 9 shows the transfer free energy, ΔG^*, transfer enthalpy, ΔH^*, and transfer entropy, $T\Delta S^*$ at two different temperatures, $T^* = 0.2$ (red) and $T^* = 0.3$ (green), as a function of solute size. For all three thermodynamic functions describing transfer of a hydrophobic particle, there are clearly two distinct areas of behavior, as observed experimentally [1, 2, 22–26, 49, 50]. In Figure 10, we plotted the dependence of the solvation free energy, enthalpy, and entropy on solute radius and temperature. We can see from the figure the equivalent behavior of the free energy of transfer upon increasing the temperature or decreasing the size of the nonpolar solute. Figure 11 shows 3D plots with the following temperature and size dependent fits through the points:

$$\Delta G^* = -7.47906 * T^* + 1.20461 * \sigma_s^* + 1.45645 \tag{31}$$

$$\Delta H^* = -4.1216 * T^* + 1.02603 * \sigma_s^* + 0.4797 \tag{32}$$

$$T\Delta S^* = -15.1371 * T^* - 0.102591 * \sigma_s^* + 5.11875 \tag{33}$$

Figure 12 shows 3D plots with the temperature and size dependences of solute insertion thermal properties per unit surface area of the non-polar solute. Increasing temperature makes

solute insertion easier. There are two mechanisms of solvation for small and big solutes. Te figure clearly shows that the solvation free energy for large solutes increases linearly with area, while for small solutes it increases linearly with volume at all temperatures.

D. The theory predicts how nonpolar solvation depends on pressure

Figure 13 shows (a) the predicted pressure dependences of the transfer free energy, ΔG^*, (b) the transfer enthalpy, ΔH^* and (c) the transfer entropy, $T^*\Delta S^*$, for different sizes of hydrophobes. Such quantities are notoriously difficult to obtain from simulations of most atomistic models, particularly at high pressures, where it is difficult to obtain reliable results from the Widom insertion method, while our theory can easily calculate these properties. The theory predicts that the free energy of solvation for small solutes becomes linearly more unfavorable with pressure, while the enthalpy and entropy of solvation exhibit very little pressure dependence for small solutes, consistent with experiments [51–53] and theory [54]. For bigger solutes, the situation is different. The free energy of solvation increases more strongly with increased pressure, while the entropy and enthalpy show nonmonotonic behavior, but both effects compensate.

The results above show that the present theory reproduces the thermal, volumetric and solute-size dependences of the solvation properties of nonpolar solutes rather well, compared to Monte Carlo simulations of the same model [45, 46], and both the theory and simulations give the experimentally observed trends. Disagreement becomes bigger at large solute sizes and low temperatures which might be either a problem of the theory or incomplete convergence of the simulation data.

E. The solvation properties can be interpreted in terms of first-shell and bulk water bonding fractions

In this section, we give a more microscopic explanation of these properties based on the different bonding populations. Figure 14a shows the temperature dependence of the ratio, $f_j^{\rm h}/f_j$, of the population of waters forming Hbonds in the first shell around a solute, relative to the population of waters forming Hbonds in the bulk. Note that we omitted ratios of caged populations from the figure since, in most of the ranges, the individual cage population

is very close to 0 and numerical uncertainty is high when dividing with numbers close to 0. In the following, we interpret these results with increasing temperature, starting from very cold water, to cold water, to hot water. **(1) Very cold water.** The theory shows that in very cold water, the first-shell solvating waters differ from bulk waters in having more Hbonds, more vdW bonds, less empty space, and those waters are well-packed ($\langle r \rangle \approx 1$) and have low-variance, well-defined Hbond angles (Figure 14e). These first-shell waters are better structured than waters in the bulk. We are seeing a sort of stochastic version of the "iceberg" idea first proposed by Frank and Evans in 1945 [55]. The reason for this structuring is clear from the model. Hydrogen bonding is a driver of water structure. More Hbonds are formed in first shells than in the bulk because the solute restricts the Hbond angle options more than in the bulk. **(2) Cold water.** Increasing the temperature from very cold ($T^* = 0.16$) to just cold water ($T^* = 0.2$) melts out vdW interactions, slightly loosening up the water structure, supporting an *increase* in Hbonds. **(3) Hot water.** Increasing the temperature further leads to melting out first-shell water Hbonds, vdW interactions, increasing the average water spacings and increasing the variance in Hbond angles. Correspondingly, Figure 14b shows how applied pressure affects water molecules in the solvation shell relative to the bulk. Applying pressure has the following effects on solvation-shell waters, relative to bulk waters: pressure squeezes vdW-bonded water molecules together in the first shell, it squeezes out empty spaces, and it reduces the average water-water spacings in the first shell. At the same time, applying pressure increasingly breaks first-shell Hbonds, reducing the excess structure there, and reduces the Hbond angle variance.

V. CONCLUSIONS

In this work, we have developed a theory for the hydration thermodynamics of a spherical hydrophobe in 3D MB-like water. The results for transfer free energy, transfer enthalpy, transfer entropy, and transfer volume obtained by the analytical theory show good agreement with the computer simulation results for the same model for all the parameters studied. The results under these conditions are consistent with the existing experimental and theoretical results. In addition, the analytical theory enabled us to study the thermodynamics of solvation under the conditions where the computer simulation results were unreliable due to the large statistical uncertainty, namely at high pressures, low temperatures and large

solutes. Theory can easily calculate solvation properties in the supercooled region of phase space since we do not have problems with crystallization. This theory only describes liquid properties of the 3D MB water model. The present work demonstrates that that general anomalies of the hydrophobic effect – which are regarded as arising from the cage-like or network-like properties of water – can be captured in a simple theory in which water-water interactions are only treated up through 2-body nearest-neighbor effects and cooperative effects.

ACKNOWLEDGMENTS

We are grateful for the support of the NIH (GM063592) and Slovenian Research Agency (P1 0103-0201, N1-0042) and the National Research, Development and Innovation Office of Hungary (SNN 116198).

[1] Tanford, C. *The hydrophobic effect: formation of micelles and biological membranes*; John Wiley & Sons, Inc: New York, 1973.

[2] Ben-Naim, A. *Solvation Thermodynamics*; Plenum Press: New York, 1987.

[3] Lazaridis, T. *Hydrophobic Effect*; In: eLS. John Wiley & Sons, Ltd: Chichester, 2013.

[4] W. Kauzmann, Adv. Protein Chem. **14**, 1 (1959).

[5] F. H. Stillinger, J. Solution Chem. **2**, 141 (1973).

[6] D. E. Smith and A. D. J. Haymet, J. Chem. Phys. **98**, 6445 (1993).

[7] M. Kanduc, A. Schlaich, E. Schneck and R. R. Netz, Langmuir **32**, 8767 (2016).

[8] D. Ben-Amotz, Annual Review of Physical Chemistry **67**, 617 (2016).

[9] T. Urbic and K. A. Dill, J. Chem. Phys. **132**, 224507 (2010).

[10] T. Urbic, Phys. Rev. E. **85**, 061503 (2012).

[11] T. Urbic, Phys. Rev. E. **94**, 042126 (2016).

[12] M. Luksic, T. Urbic, B. Hribar-Lee and K. A. Dill, J. Phys. Chem. B **116**, 6177 (2012).

[13] N.T. Southall and K. A. Dill, J. Phys. Chem. B. **104**, 1326 (2000).

[14] N.T. Southall, K. A. Dill and A. D. J. Haymet, J. Phys. Chem. B. **106**, 521 (2002).

[15] K. A. Dill, Biochemistry **29**, 7133 (1990).

[16] D. Chandler, Nature **437**, 640 (2005).

[17] K. Lum, D. Chandler, J. D. Weeks, J. Phys. Chem. B **103**, 4570 (1999).

[18] D. M. Huang, D. Chandler, J. Phys. Chem. B **106**, 2047 (2002).

[19] D. M. Huang, P. L. Geissler, and D. Chandler, J. Phys. Chem. B **105**, 6704 (2001).

[20] H. Reiss, H. L. Frisch and J. L. Lebowitz, J. Chem. Phys. **31**, 369 (1959).

[21] L. R. Pratt and D. Chandler, J. Chem Phys. **67**, 3683 (1977).

[22] R. Crovetto, R. FernandezPrini, M. L. Japas, J. Chem. Phys. **76**, 1077 (1982).

[23] D. R. Biggerstaff, R. H. Wood, J. Phys. Chem. **92**, 1988 (1988).

[24] D. R. Biggerstaff, R. H. Wood, J. Phys. Chem. **92**, 1994 (1988).

[25] A. Ben-Naim, Y. Marcus, J. Chem. Phys. **80**, 4438 (1984).

[26] A. Ben-Naim, Y. Marcus, J. Chem. Phys. **81**, 2016 (1984).

[27] A. Bizjak, T. Urbic, V. Vlachy, and K. A. Dill, Acta Chim. Slov. **54**, 532 (2007).

[28] K. A. T. Silverstein, A. D. J. Haymet, K. A. Dill, J. Am. Chem. Soc. **120**, 3166 (1998).

[29] M. Huš and T. Urbic, J. Chem. Phys. **140**, 144904 (2014).

[30] S. V. Buldyrev, P. Kumar, P. G. Debenedetti, P. J. Rossky and H. E. Stanley, Proc Natl Acad Sci U S A, **104**, 20177 (2007).

[31] T. Head-Gordon, Chem. Phys. Letts. **227**, 215 (1994).

[32] M. Jochum, D. Andrienko, K. Kremer and C. Peter, J. Chem. Phys. **137**, 064102 (2012).

[33] A. Ben-Naim, J. Chem. Phys. **54**, 3682 (1971).

[34] A. Ben-Naim, Mol. Phys. **24**, 705 (1972).

[35] A. Ben-Naim, *Water and Aqueous Solutions* (Plenum Press, New York, 1974).

[36] A. Ben-Naim, *Molecular Theory of Water and Aqueous Solutions, 1st ed.* (World Scientific, Singapore, 2009).

[37] A. Bizjak, T. Urbic, V. Vlachy and K. A.Dill, J. Chem. Phys. **131**, 194504 (2009).

[38] C. L. Dias, T. Ala-Nissila, M. Grant and M. Karttunen, J. Chem. Phys. **131**, 054505 (2009).

[39] C. L. Dias, T. Hynninen, T. Ala-Nissila, A. S. Foster and M. Karttunen, J. Chem. Phys. **134**, 065106 (2011).

[40] E. A. Jagla, J. Chem. Phys. **111**, 8980 (1999).

[41] T. M. Truskett and K. A. Dill, J. Chem. Phys. **117**, 5101 (2002).

[42] T. M. Truskett and K. A. Dill, J. Phys. Chem. B **106**, 11829 (2002).

[43] L. E. Coronas, V. Bianco, A. Zantop and G. Franzese, arxiv:1610.00419v1

[44] H. Xu and K. A. Dill, J. Phys. Chem. B **109**, 23611 (2005).

[45] T. Mohoric, T. Urbic and B. Hribar-Lee, J. Chem. Phys. **139**, 024101 (2013).

[46] T. Mohoric, T. Urbic and B. Hribar-Lee, J. Chem. Phys. **140**, 024502 (2014).

[47] A. Chaimovich and M. S. Shell, Phys. Rev. E **88**, 052313 (2013).

[48] A. Chaimovich and M. S. Shell, Phys. Rev. E **89**, 022140 (2014).

[49] M. H. Abraham, P. L. Grellier, R. A. McGill, J. Chem. Soc. Perkin Trans. II, 797 (1987).

[50] M. H. Abraham, P. L. Grellier, R. A. McGill, J. Chem. Soc. Perkin Trans. II, 339 (1988).

[51] W. L. Masterton, J. Chem. Phys. **22**, 1830 (1954).

[52] T. R. Rettich, Y. P. Handa, R. Battino, E. Wilhelm, J. Phys. Chem **85**, 3230 (1981).

[53] L. Hnedkovsky, R. H. Wood, J. Chem. Thermodynamics **29 1997**, 731 (1997).

[54] M. S. Moghaddam, H. S. Chan, J. Chem. Phys. **126**, 114507 (2007).

[55] H. S. Frank and M. W. Evans, J. Chem. Phys. **13**, 507 (1945).

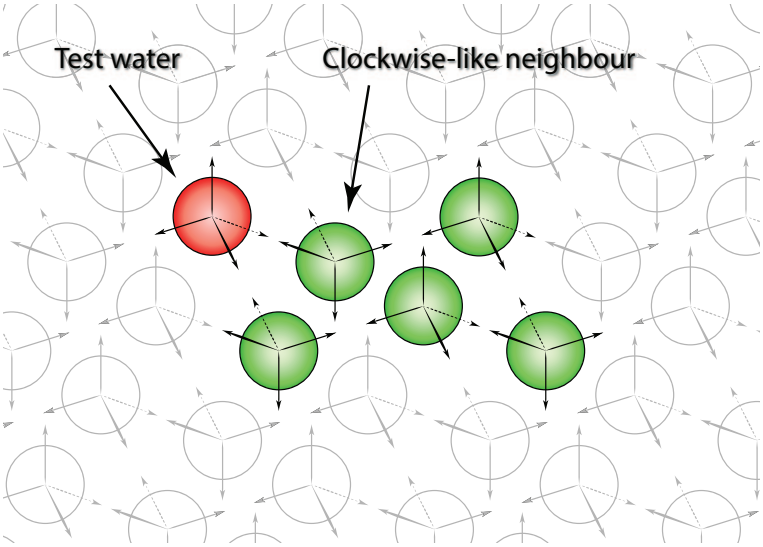

Figure 1 (Urbic et al.)

Figure 1. The test water molecule in the context of its water lattice. It shows the principal pair neighbor interaction, taken clockwise, to avoid triple counting.

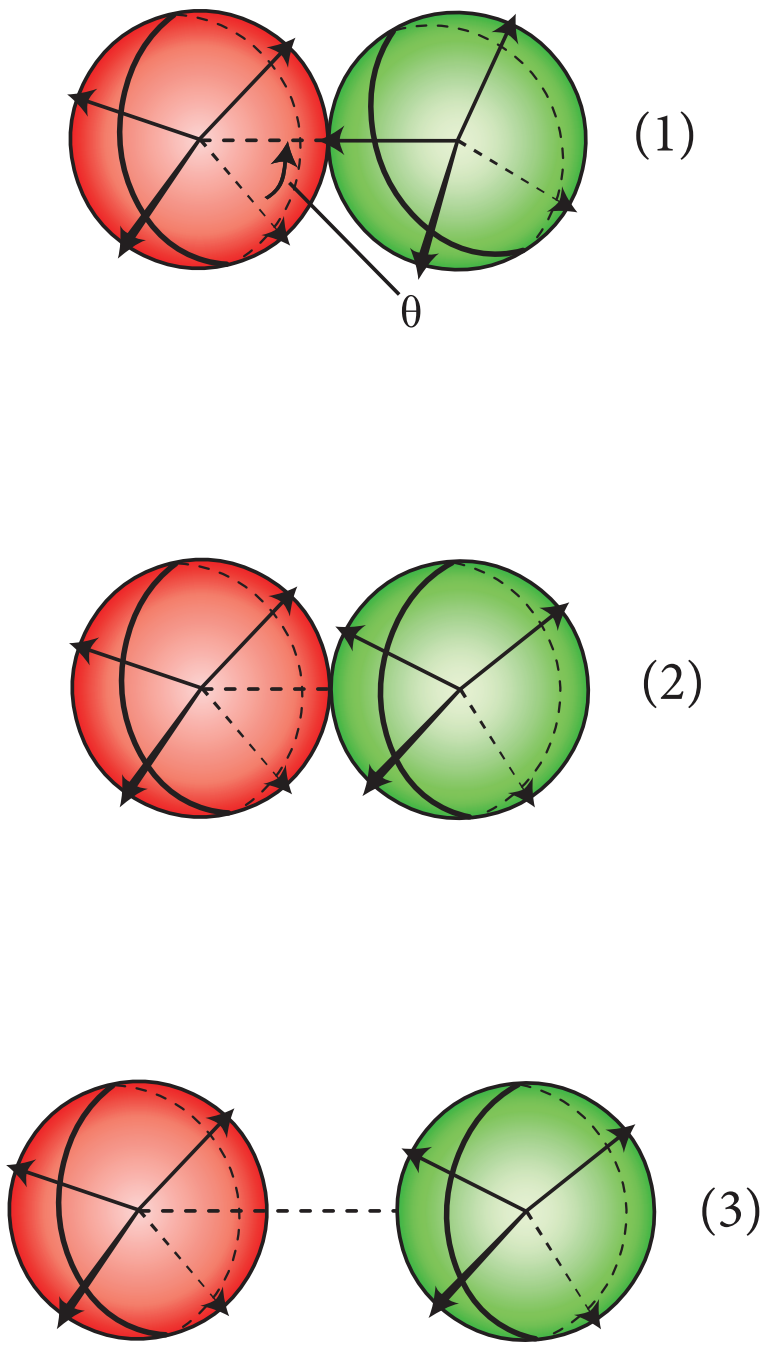

Figure 2 (Urbic et al.)

Figure 2. The three states that define pairwise water-water interactions: (1) hydrogen-bonded, (2) Lennard-Jones-bonded (LJ) pairs (no Hbond), or (3) nonbonded (having neither an Hbond or LJ bond).

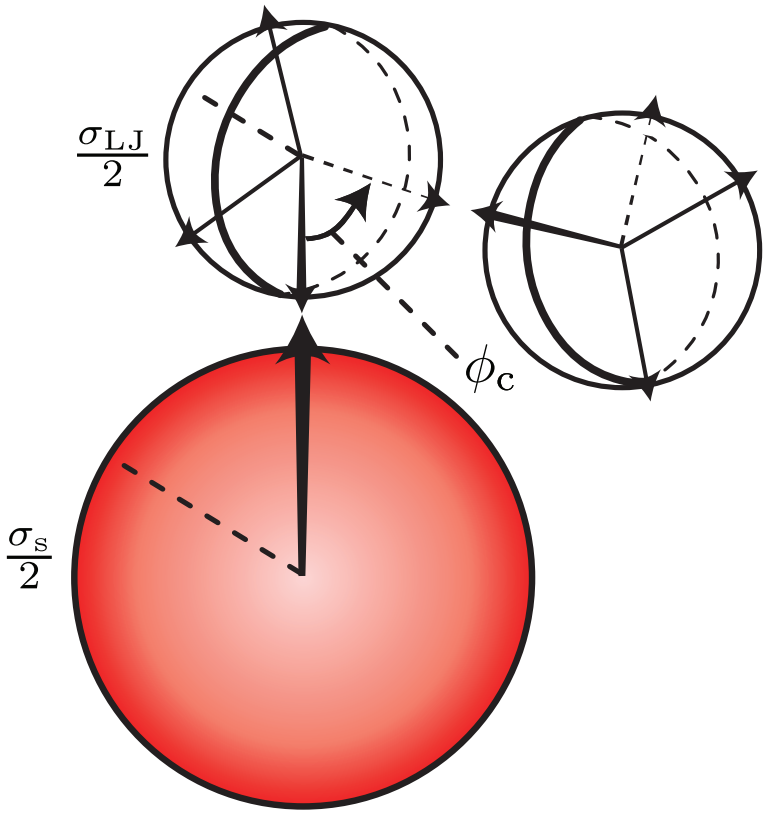

Figure 3 (Urbic et al.)

Figure 3. Definition of the critical angle, ϕ_c

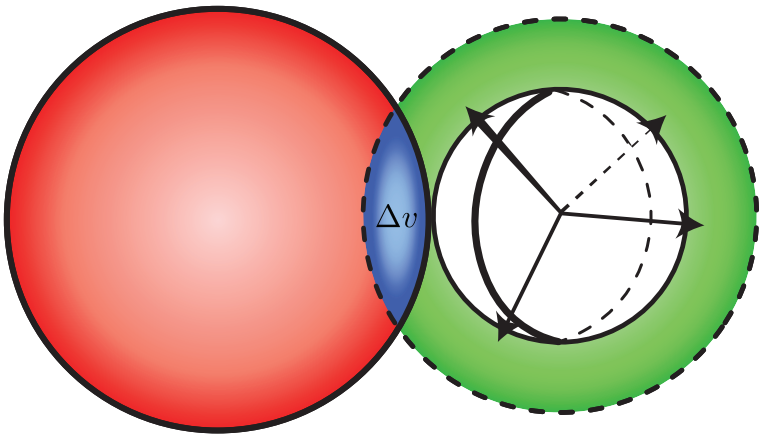

Figure 4 (Urbic et al.)

Figure 4. Definition of the overlap volume, Δv.

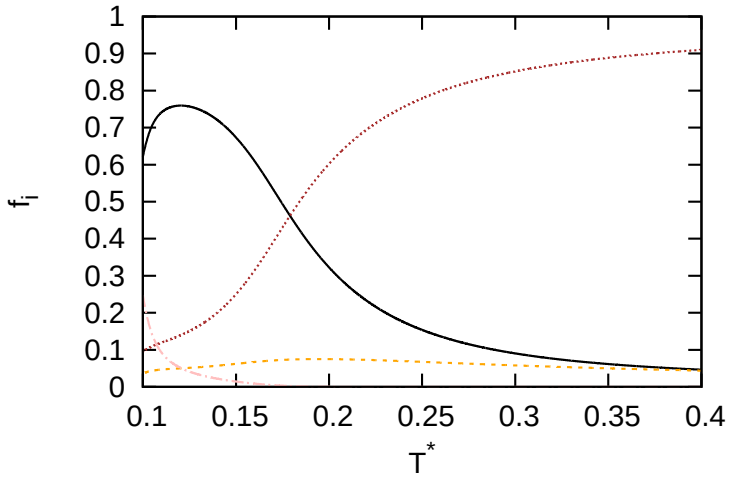

Figure 5 (Urbic et al.)

Figure 5. The computed pairwise bulk populations f_j *vs.* temperature, at $p^* = 0.12$. (Black) Hbonded water population. (Orange) LJ population. (Red) Nonbonded population. (Pink) HB cage population. It shows the melting out of Hbonded structure with temperature in the bulk, and its replacement by nonbonded.

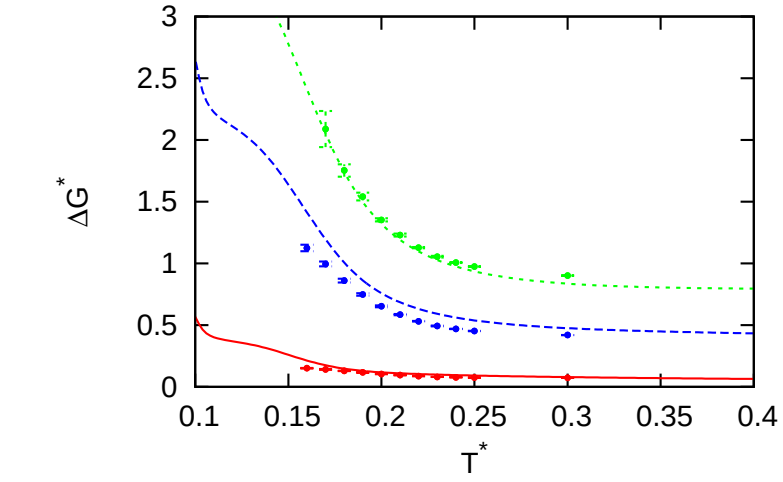

(a)

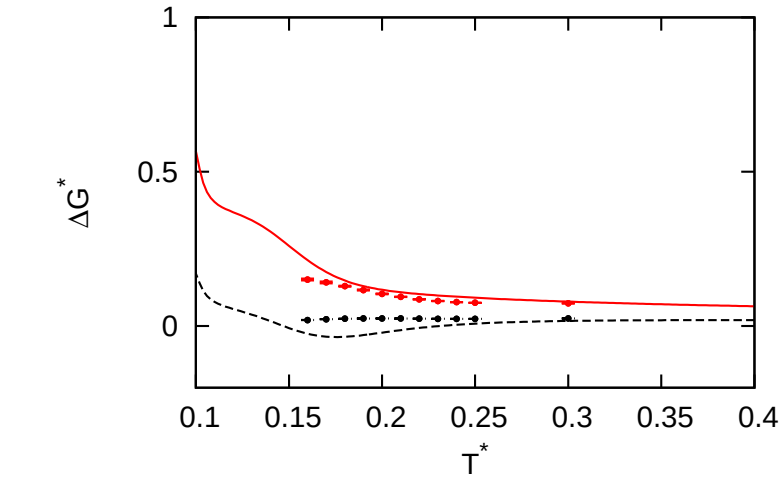

(b)

Figure 6 (Urbic et al.)

Figure 6. Transfer free energy, ΔG^*, into water of solutes of different radii. (a) Large solutes: $\sigma_S^* = 0.7$ (red), $\sigma_S^* = 1.5$ (blue), $\sigma_S^* = 2.0$ (green). (b) Smaller solutes: $\sigma_S^* = 0.3$ (black), $\sigma_S^* = 0.7$ (red). Lines show the theory and points show the Monte Carlo results. The larger solutes are most opposed to dissolving, and this effect weakens upon heating.

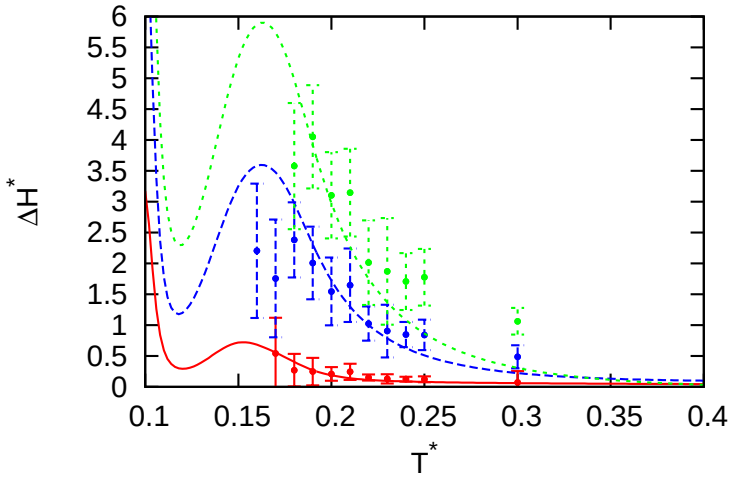

(a)

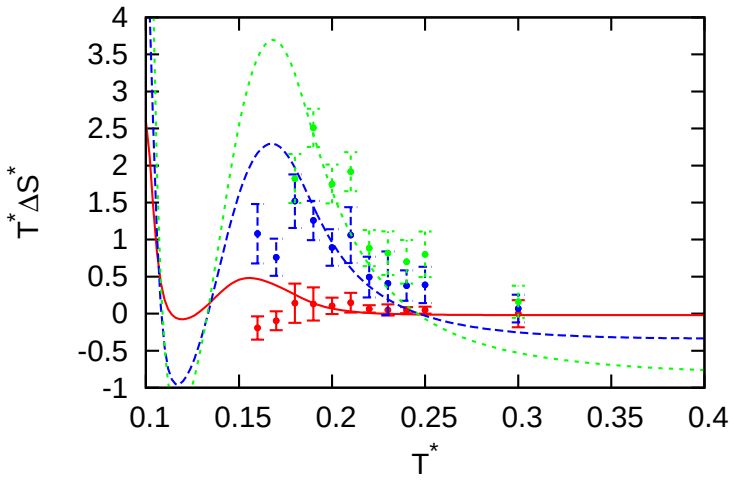

(b)

Figure 7 (Urbic et al.)

Figure 7. Transfer enthalpy ΔH^* and entropy $T^*\Delta S^*$ into water of large solutes of different radii, for $\sigma_S^* = 0.7$ (red), $\sigma_S^* = 1.5$ (blue), $\sigma_S^* = 2.0$ (green). Lines show the theory and points give the Monte Carlo results. There is substantial enthalpy-entropy compensation.

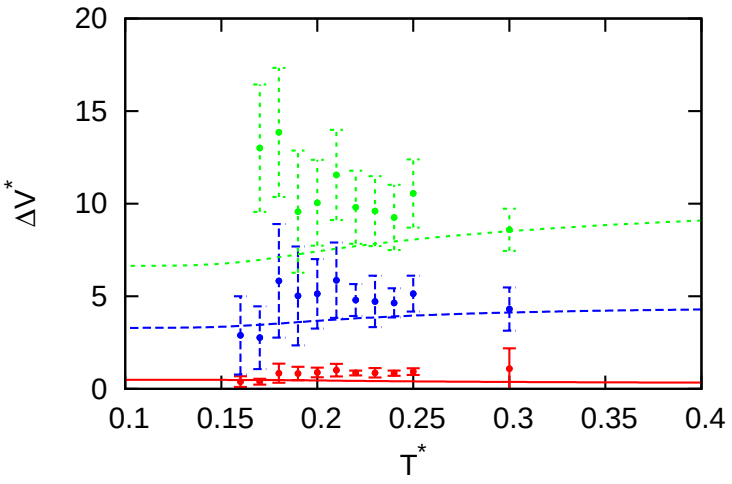

Figure 8 (Urbic et al.)

Figure 8. Transfer volume, ΔV^*, as a function of temperature, for $\sigma_S^* = 0.7$ (red), $\sigma_S^* = 1.5$ (blue), $\sigma_S^* = 2.0$ (green). Not surprisingly, larger solutes have larger excess volumes of insertion. Lines show theoretical results and points Monte Carlo results.

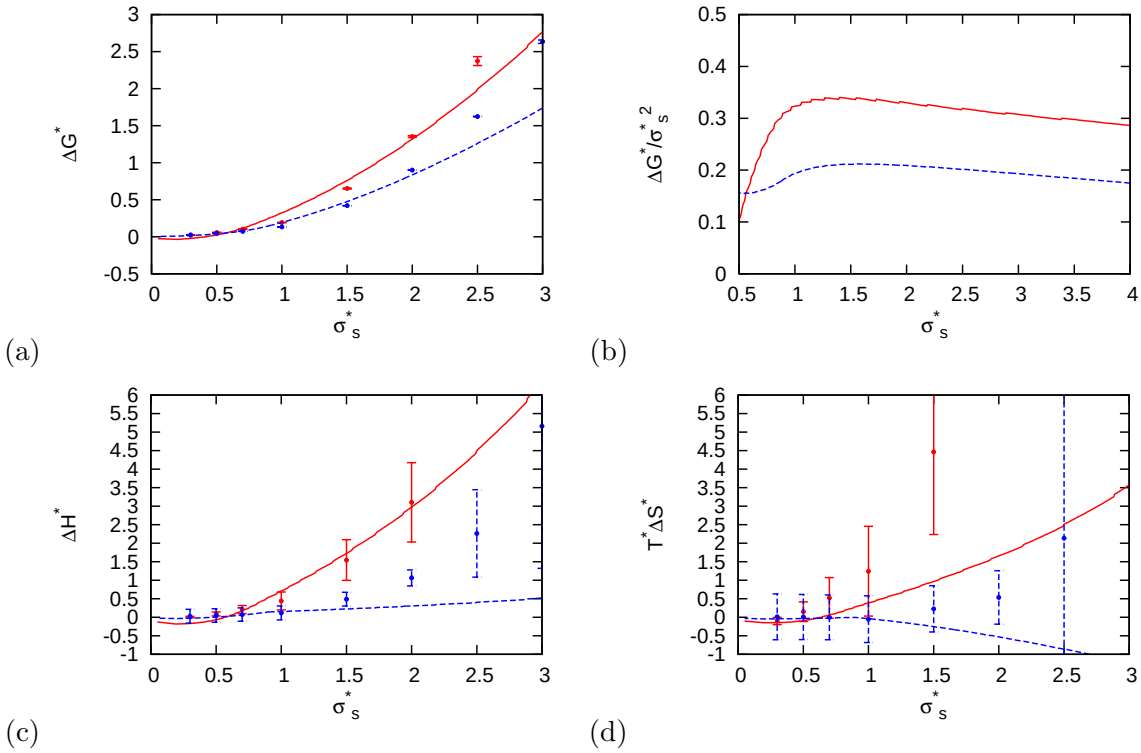

Figure 9 (Urbic et al.)

Figure 9. How the solute insertion thermodynamics depends on solute radius. (a) Transfer free energy, ΔG^*, (b) transfer free energy per unit surface area of the non-polar solute, (c) transfer enthalpy, ΔH^*, and (d) transfer entropy, $T^*\Delta S^*$, as a function of hydrophobe size (σ_S^*) at two different temperatures: $T^* = 0.2$ (red) and $T^* = 0.3$ (blue) at $p^* = 0.12$. Larger solutes are more expensive to insert for enthalpy reasons, but are entropically favored in cold water and disfavored in hot water. Points are Monte Carlo results and lines are theoretical results.

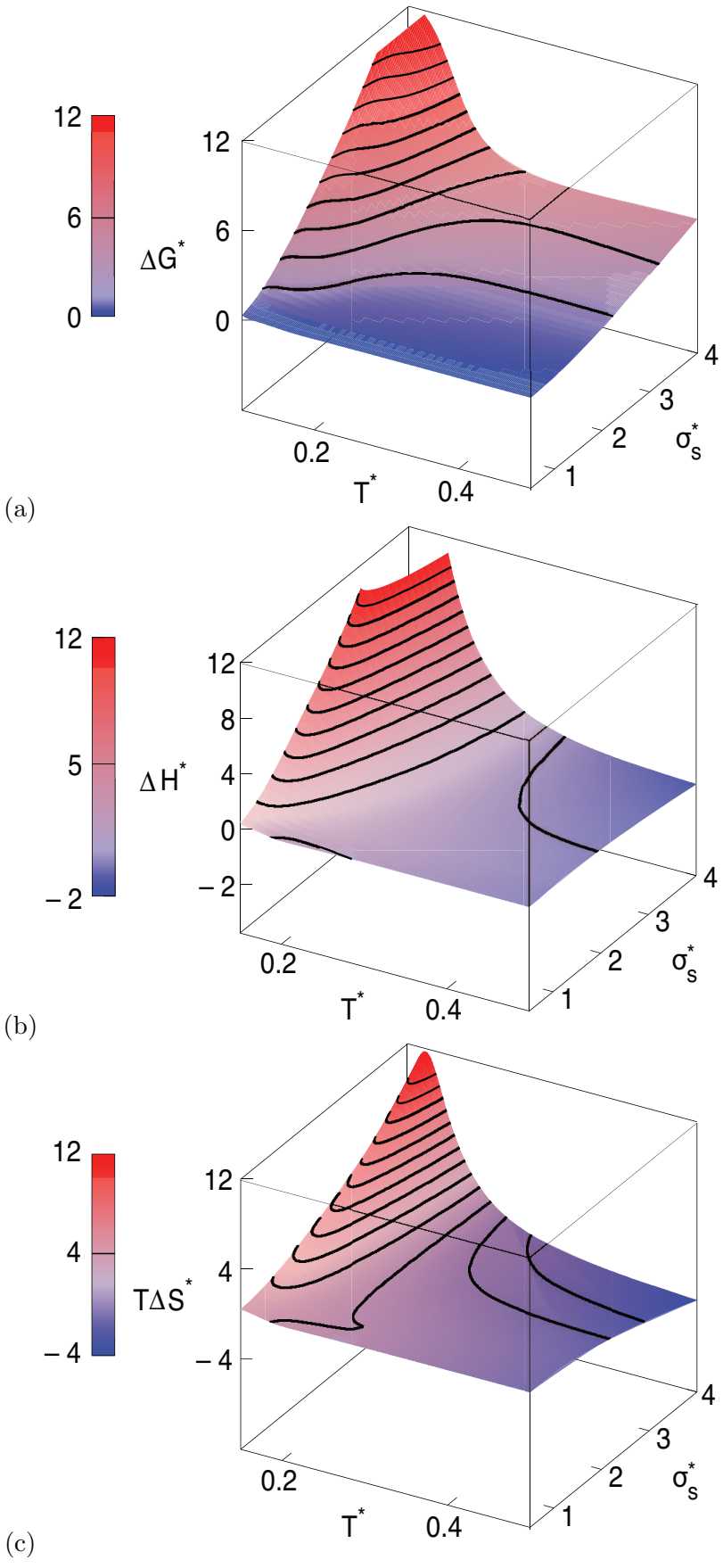

Figure 10 (Urbic et al.)

Figure 10. Solute insertion thermal properties *vs.* both temperature and solute radius.

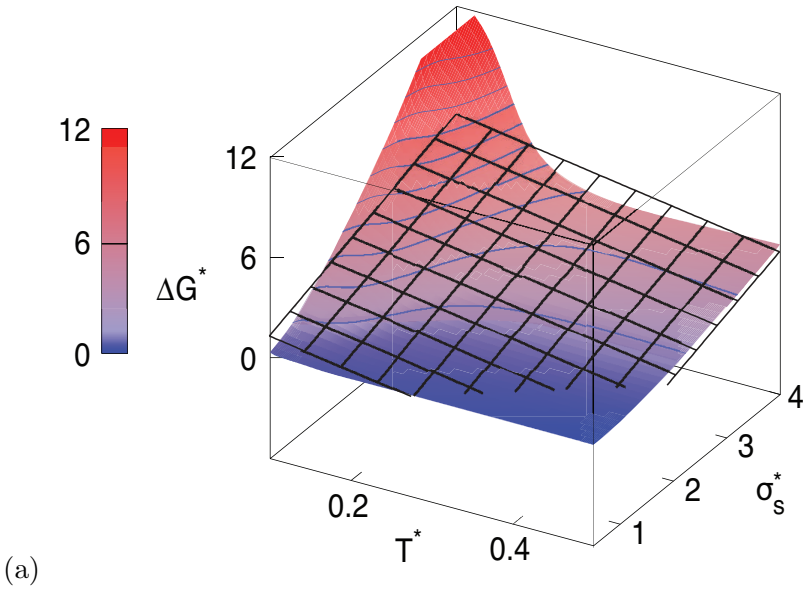

(a)

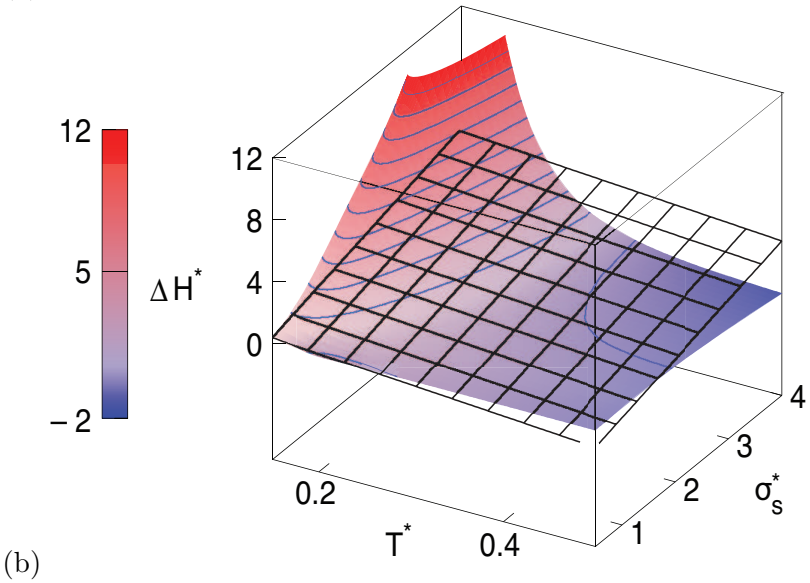

(b)

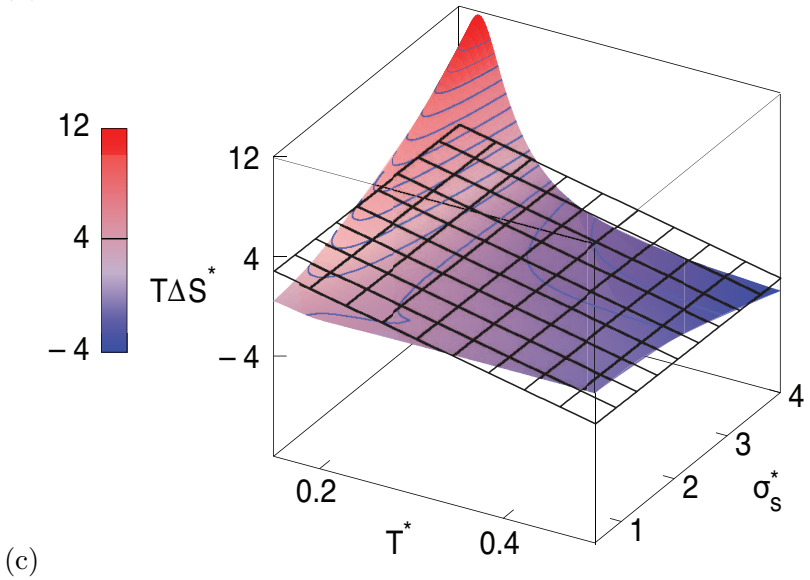

(c)

Figure 11 (Urbic et al.)

Figure 11. Same as figure 10, but also showing a plane indicating linear fits in both variables in

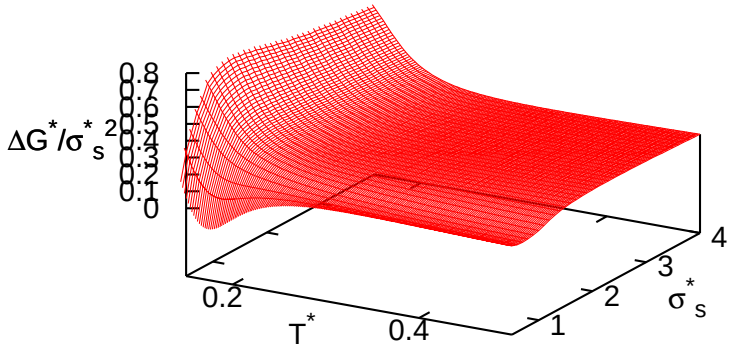

(a)

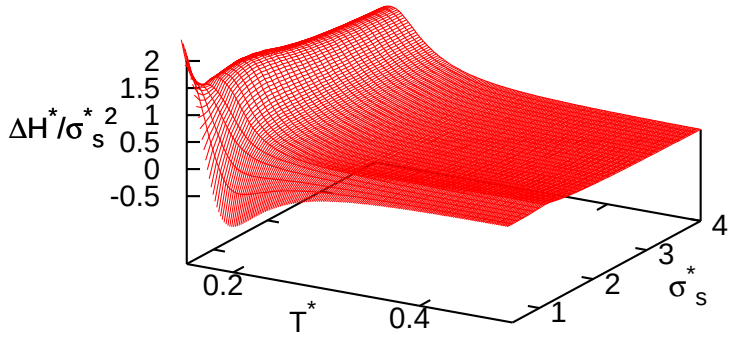

(b)

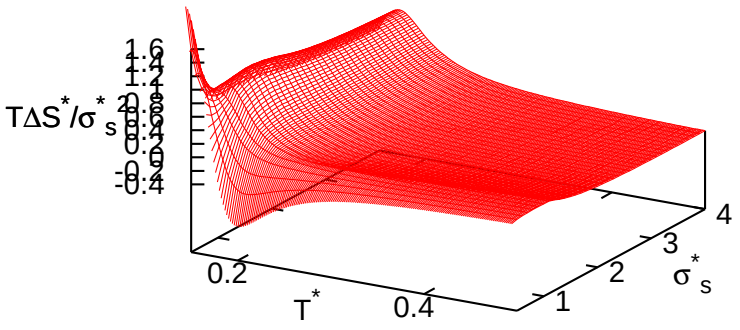

(c)

Figure 12 (Urbic et al.)

Figure 12. Solute insertion thermal properties per unit surface area of the non-polar solute *vs.* both temperature and solute radius. Increasing temperature makes solute insertion easier. There are two mechanisms of solvation for small and big solutes.

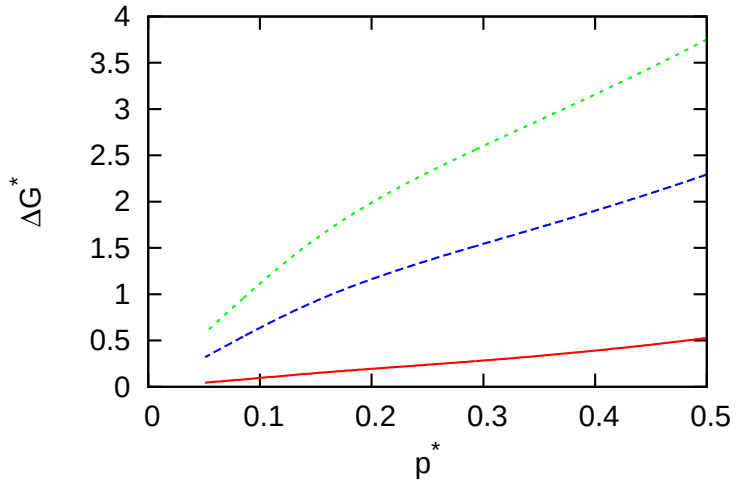

(a)

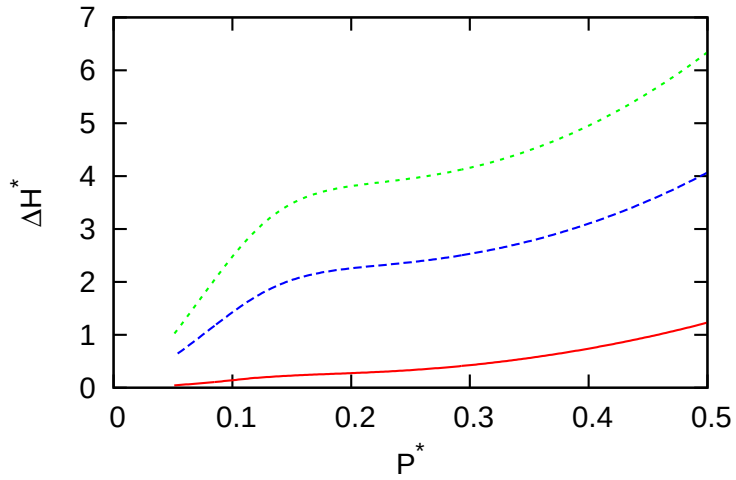

(b)

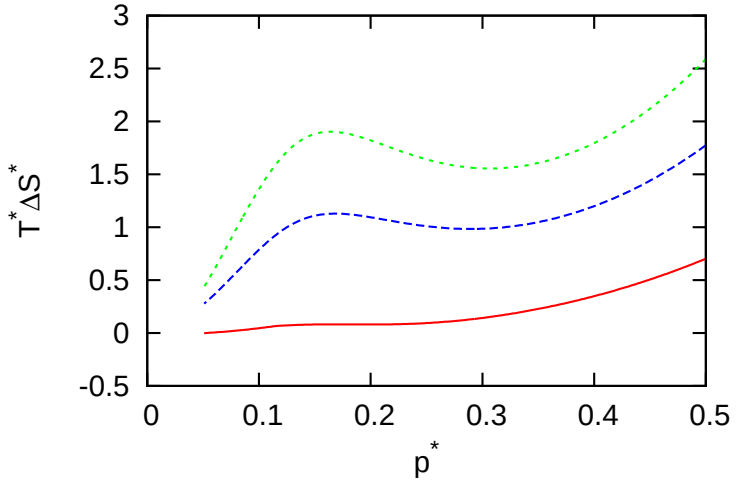

(c)

Figure 13 (Urbic et al.)

Figure 13. Pressure dependences of solute transfer thermal quantities, for solute sizes $\sigma_S^* = 0.7$ (red), $\sigma_S^* = 1.5$ (blue), $\sigma_S^* = 2.0$ (green). Applying pressure squeezes the space available, making solute insertion more difficult. There is enthalpy - entropy compensation.

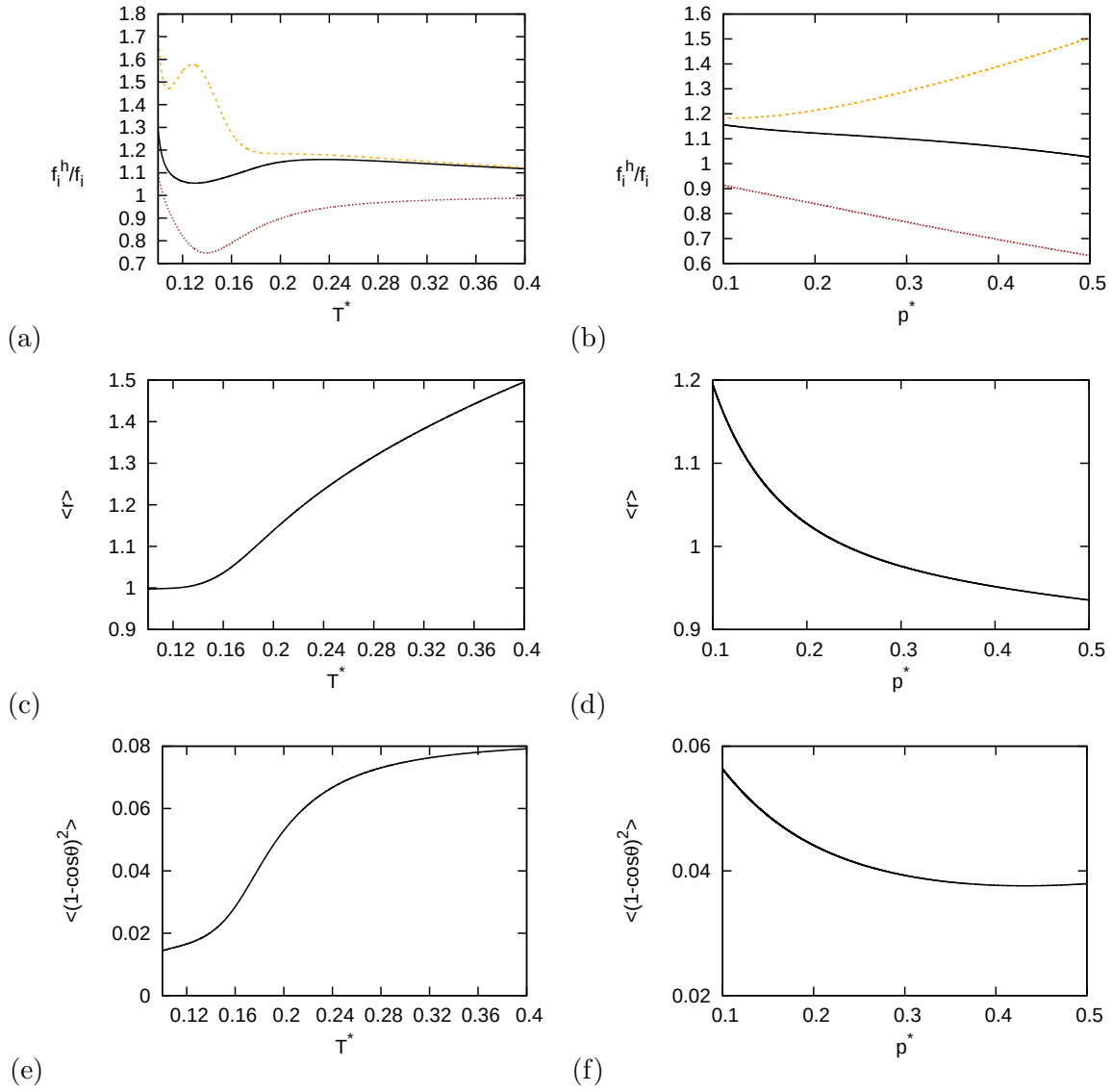

Figure 14 (Urbic et al.)

Figure 14. Molecular structure properties *vs.* temperature and pressure for (a) $p^* = 0.12$ and (b) $T^* = 0.2$. (Top row) Ratio f_j^{h}/f_j of populations of first-shell to bulk waters: (Black) Hbonded waters, (Orange) LJ waters, (Red) Nonbonded waters. This shows that the shell has more Hbonding and LJ bonds than the bulk, and that shell Hbonds melt out faster with increasing temperature than bulk Hbonds do. It shows that the first shell is better packed (fewer NB waters). (Middle row) $\langle r \rangle$ is the average separation between waters. Heating warm water increases the water-water separations. At all temperatures, pressure pushes waters closer together. (Bottom row) $\langle (1-\cos\theta)^2 \rangle$ is the variance in Hbond angles, a measure of 'bending flexibility'. Heating increases this variance, while pressure decreases it.